J MATER SCI 41 (2006) 1711–1720

The effect of shock-loading on the aging behavior of an Al-Mg-Si alloy

R. S. YASSAR
School of Mechanical and Materials Engineering, Washington State University, Pullman, WA 99164-2920, USA

M. CAI
Physics department, Washington State University, Pullman, WA 99164, USA

D. P. FIELD*
School of Mechanical and Materials Engineering, Washington State University, Pullman, WA 99164-2920, USA
E-mail: field@mme.wsu.edu

X. CHEN, J. ASAY
Institute of Shock Physics, Washington State University, Pullman, WA 99164, USA

Published online: 17 February 2006

The impact of pre-shock loading on the precipitation reactions in an Al-Mg-Si alloy (AA6022) was studied by means of differential scanning calorimetry (DSC), transmission electron microscopy (TEM) and hardness measurements. The samples were solutionized and quenched in water prior to subsequent shock-loading and aging treatment. The TEM and DSC results show that, while shock-loading prior to aging facilitated the precipitation of Q' and β, no significant effect on β'' precipitates was observed. The hardness studies indicate that pre-shock loading strengthens the material by forming a high concentration of microstructural defects, however the resultant mechanical properties of the shocked sample are comparable to those without shock processing at the peak of aging. It was found that the rate of overaging is higher in shocked samples, which is in agreement with the DSC and TEM results.

1. Introduction

The relationship between intense shock compression and material defects has had a long history, dating back to the early work [1] who proposed a specific mechanism for the generation of dislocations occurring at moving shock discontinuities. Early work on dynamic yielding resulting in elastic precursor decay ([2]) illustrated the significant effects of small preexisting concentrations of divalent impurities on dynamic yield processes in single crystal LiF. Generally, it is known that shock-loading produces a large number and variety of distributed defects in solids, including dislocations, stacking faults, and twins. An extensive literature has been developed dealing with the effects of shock-loading on the production of these various defects that are known to influence mechanical properties such as quasi-static loading. It is not appropriate to discuss this previous work in the present paper; the reader is directed to a few selected references for further information on the topic ([3–7]). In contrast to the general studies of shock-induced defects, there are relatively few reports dealing with the effect of shock-loading on the specific issue of aging properties resulting after shock-loading. Recent papers on this issue include the work [8] on the characterization of a shock-loaded aluminum alloy [9] on the effect of shock-wave prior to the aging of austenitic stainless steels [10] on studies of aging processes in shocked aluminum alloys.

In spite of a limited number of studies on the combination of shock-loading and aging response of aluminum alloys, apparently no detailed analyses are available on the effect of shock-loading on the evolution of precipitation structures of these alloys during aging. In contrast, extensive studies on the precipitation sequence of aluminum alloys without shock-loading are available in the litera-

*Author to whom all correspondence should be addressed.
0022-2461
DOI: 10.1007/s10853-006-2933-z

ture e.g. [11–13]. In general, the age-hardening response of Al-Mg-Si alloys is based on the precipitation reactions. A widely accepted precipitation sequence in these alloys is:

$$\alpha(\mathrm{SSSS}) \rightarrow \text{Clusters/GP zones} \rightarrow \beta'' \rightarrow \beta' \rightarrow \beta$$

Atomic clusters of Mg and Si and GP zones are believed to form at an early stage of precipitation from supersaturated Al-Mg-Si aluminum alloy [11–13]. Their existence has been confirmed by means of three dimensional atom probe analyses (3DAP) [12]. The β'' are fine needle-shaped precipitates along $<100>_{\mathrm{Al}}$, and have monoclinic structure [14]. Maximum hardness can be achieved when β'' dominates the precipitates in the material. The β' precipitates with hexagonal crystal structure form after β'' precipitates in the aging sequence [15]. They are rod-shaped and are aligned along $<100>_{\mathrm{Al}}$. In Al-Mg-Si alloys, the equilibrium β-phase has antiflourite FCC structure with lattice parameter of 0.639 nm [16].

This paper aims to investigate the effect of shock-loading on the precipitation sequence during dynamic aging and isothermal aging of an Al-Mg-Si alloy. It is expected that the production of a high and uniform concentration of microstructural defects due to shock-loading influence the aging response of the material. In this work systematic transmission electron microscopy (TEM) and differential scanning calorimetry (DSC) experiments were performed to characterize the evolution of precipitate structures as well as aging response of an Al-Mg-Si alloy.

2. Experimental procedure

Aluminum alloy 6022 (AA6022) with the composition of 0.55%Mg-1.10%Si-0.07wt%Cu was received in thin plate form with a thickness of 3.50 mm. Solution treatment was carried out at 550°C for 1 h with a programmable furnace and then water-quenched to room temperature. The samples were then preserved at 0°C before further experiments.

A schematic of the impact test and soft recovery configuration of samples is shown in Fig. 1, which is based on designs previously developed [17, 18]. For experiments of shock-induced aging effects, 6022 aluminum samples were machined in the form of disks, 50.8 mm in overall diameter and 3.07 mm in thickness. Each sample studied was prepared in two pieces. The inner piece was 25.4 mm in diameter with a beveled edge on the outer diameter of 8 deg to the normal. The outer ring had a matching bevel angle to accommodate the inner piece with a tight press fit between the inner diameter of the ring and the central piece. The bevel angle direction was chosen, as illustrated in Fig. 1 to allow quick separation of the central aluminum sample from the aluminum guard ring after first shock passage and consequent unloading upon reflection for the shock wave from the back surface (right side in Fig. 1) of the sample assembly. The inner diameter was designed so that after the central piece is fully unloaded, the inward moving radial release waves would cause a separation of the two pieces, resulting in a central piece which was only loaded and unloaded with planar stress waves. The pieces were bonded together with a molybdenum lubricant to minimize perturbations caused by the shock wave at this interface. To produce the desired impact stress, the sample was impacted by a flat disk of aluminum accelerated to the velocity of 292 m/s. A measured planar impact stress of about 2.3 GPa was produced upon initial impact and maintained for a time duration of about 1 μs before planar unloading by shock reflection from the back free surface of the sample. Immediately after the shock wave experiment, the sample was recovered from the recovery fixture and placed in a liquid nitrogen bath for further metallurgical examination.

To perform DSC experiments, the shock loaded samples were grinded on both surfaces to the thickness of 0.5 mm and then punched into 3 mm disks. The average weight of the DSC samples was 9.4 ± 0.3 mg. The Rheometric Scientific$^{\mathrm{TM}}$ DSC instrument was used for calorimetric analyses. A protective atmosphere of pure argon at the rate of 11 ml/min was passed through the cell to avoid materials oxidation during the experiment. To study the precipitation sequence in the alloy, the shocked and un-shocked samples were subjected to a heating rate of 10°C/min up to a temperature of 550°C. This procedure

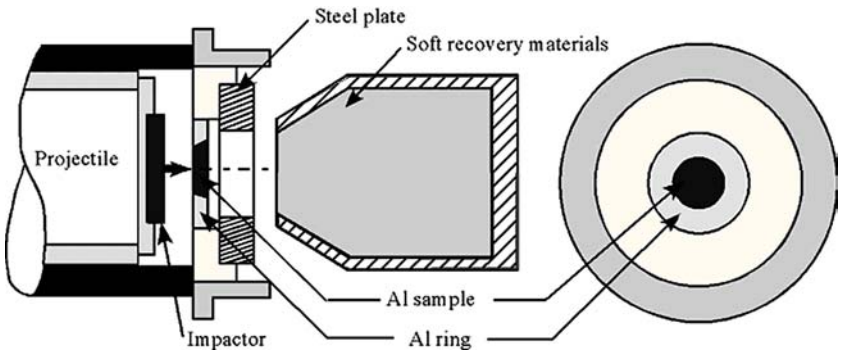

Figure 1 Experimental configuration used for shock-loading and soft recovery of aluminum samples shocked to about 2.3 GPa. The inside of the soft recover fixture was filled with absorbent materials to minimize secondary loading of the recovered aluminum sample after impact and release from the guard ring.

was repeated for several samples and a good reproducibility in the plotted DSC curves was observed. To characterize the microstructural evolution during the DSC tests, samples for TEM analyses were prepared by heating in the DSC machine with the same heating profile used during the DSC experiments. Samples were removed from the DSC apparatus and immediately quenched in cold water subsequent to achieving the temperature at which each peak in the DSC curves was observed.

To study the precipitate evolution during isothermal aging, the shocked samples were grinded on both surfaces to a total thickness of 0.5 mm and then were aged at 175°C in a salt bath furnace for various periods of time. Vickers-micro hardness and TEM studies were performed on the aged samples. Hardness measurements were conducted with a 500 g load. The hardness data were determined from the average of at least four readings from each sample.

TEM specimens were prepared by twin jet electropolishing unit in a solution of 30 (vol.)% HNO_3 and 70 (vol.)% Methanol at -20 ± 5°C and 12 VDC. TEM investigation was conducted in a Philips CM200 microscope operating at 200 keV. The selected area diffraction patterns (SADs) and dark field (DF) images were analyzed in the exact <100> zone axis orientation. Due to the strong contrast of dislocations and precipitates, it was very difficult to carefully analyze the precipitate structures (especially precipitate cross sections) in the exact <100> zone axes of Aluminum. Therefore the bright field images were obtained by tilting the sample holder less than 2° away from <100> aluminum zone axes.

3. Results and discussion

Fig. 2 shows the DSC thermogram for the as-quenched sample, heated to 550°C at a heating rate of 10°C/min. Four exothermic and one endothermic peaks were detected in the DSC and marked along the curve in sequence. The overall shape of the DSC curve is similar to those published in the literature on similar alloys [19, 20].

The clustering of Mg, Si and Mg-Si atoms and GP zone formation at the early stage of precipitation in Al-Mg-Si

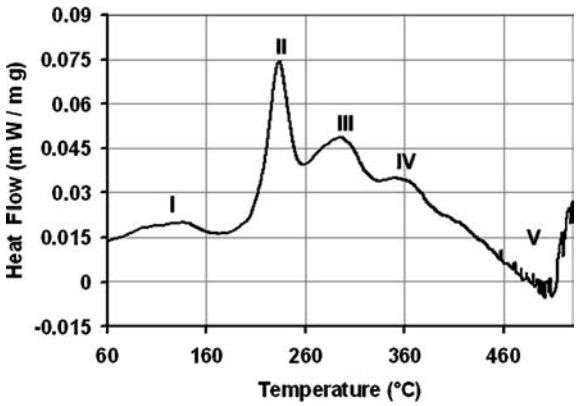

Figure 2 DSC thermogram of the as-quenched sample taken at a heating rate of 10°C/min.

alloys has been studied recently and their existence has been proven by 3DAP and high resolution TEM analysis [12–13]. Due to the blocky shape of the GP zones in Al-Mg-Si alloys, streaking from GP zones would not be expected to occur in diffraction pattern analyses. In addition, the atomic scattering factors of these three elements are very close to each other. Therefore it is difficult to resolve these zones by conventional TEM imaging. Thus, the exothermic peak I can be due to the formation of clusters/GP zones during heating of the as-quenched samples. Furthermore the temperature range for the formation of GP zones is consistent with previous studies on alloys with similar chemical composition [13, 19, 20]. For example, Miao and Laughlin [19] reported the temperature range of 60–120°C for the formation of clusters/GP zones in AA6022. Therefore as for previous reports, peak I is presumed to be due to formation of atomic clusters and GP zones.

The TEM micrographs corresponding to the samples heated just above peaks II, III and IV in Fig. 2 are shown in Figs. 3–5 respectively. Fig. 3 shows the bright field (BF) TEM micrograph and selected area diffraction (SAD) pattern of the alloy heated to 230°C (peak II). The needle-shaped precipitates are distributed homogenously in the matrix with their long axis parallel to $[100]_{Al}$ and the dark spots are needles pointing in the viewing direction (Fig. 3a). The SAD pattern shows faint streaks along $[010]_{Al}$ and $[001]_{Al}$ due to needle-like precipitates (Fig. 3b). The streaks seen in the diffraction pattern of Fig. 3b agree well with the diffraction pattern for β'' observed by Miao and Laughlin [19] and Murayama *et al.* [21]. Close examination of the end-on precipitates shows that in addition to the β'' precipitates, small lath-shaped precipitates are also present, as shown at higher magnification in the upper part of Fig. 3a. According to Chakrabarti and Laughlin [22] the habit plane and orientation relations of the lath-shaped precipitates at the late stage of overaging resembled that of Q', while they were different for the lath precipitates at early stages, thus indicating that they were possible precursors to the Q' phase. Fig. 4a shows the bright field TEM image of the precipitates after the occurrence of peak III. The diffraction pattern (Fig. 4b) and its analyses [19] (Fig. 4c), and close examination of the end-on precipitates in the bright field TEM image revealed the existence of two types of precipitates, the rectangle-shaped precipitates were present in addition to the rod-like β' precipitates. The rectangle-shaped precipitates have an angle less than 11° with the nearest $<100>_{Al}$ zone axes which agrees well with characteristics of the Q' precipitates [23]. Therefore one can conclude that that the precipitate event corresponding to peak III on the DSC trace is the simultaneous precipitation of β' and Q'. The energy dispersive spectrometry (EDS) analysis of precipitates on peak IV (Fig. 5a) determined that they are Si and Mg_2Si phases (Fig. 5b and 5c) which agrees well with results of [24]. The diffraction pattern of the region containing Mg_2Si phases and its analysis [16] is shown in Fig. 5d and 5e. The reflections other than those from the

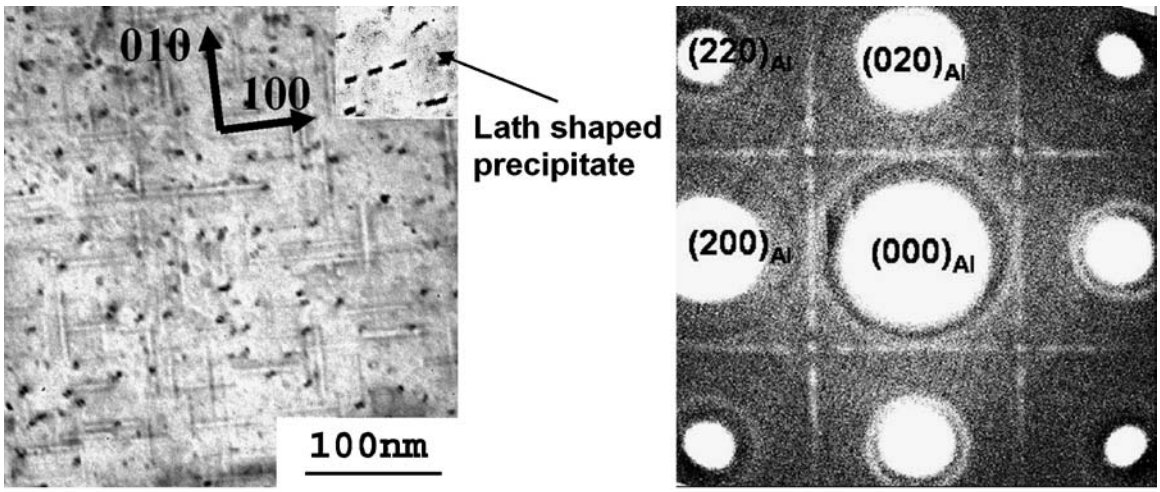

Figure 3 Microstructure of specimen heated up to peak II. (a) The needle-shaped β'' precipitates+ lath-shaped precipitates. (b) The $<100>_{Al}$ SAD pattern of microstructure in (a).

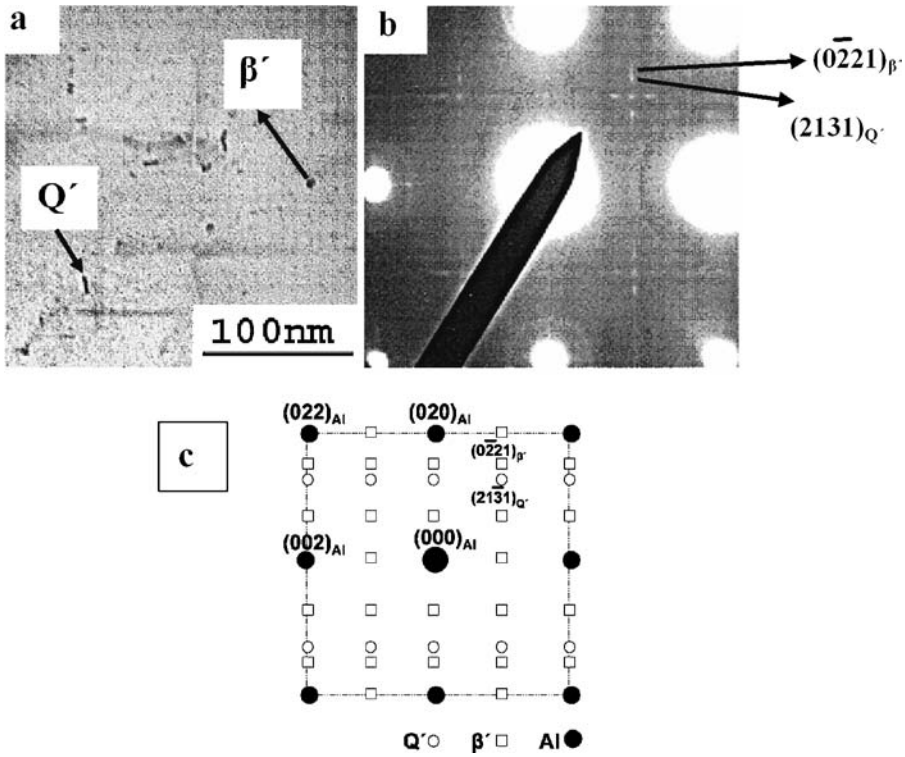

Figure 4 (a) The microstructure of the sample heated to peak III with heating rate of 10°C/min. The precipitates are either β' or Q' and are shown by arrows. (b) The <100> Al zone axes TEM diffraction pattern of microstructure (a) and its analyses (c).

Al matrix can be indexed as those from β-Mg_2Si and the double diffractions between the precipitates and the matrix are indicated by open circles in Fig. 5d. The possible origin of other reflections seen in Fig. 5d can be attributed to Si particles. The analyses of diffraction pattern indicate that the Mg_2Si particles are related to the matrix by the cube-cube orientation relationship:

$$[001]_{ß-cubes}||[001]_{Al}, \quad [100]_{ß-cubes}||[100]_{Al},$$
$$[010]_{ß-cubes}||[010]_{Al}$$

Ohmori *et al*. [16] and Westengen and Ryum [25] have also reported the formation of such cuboid precipitates in Al-Mg-Si alloys. Therefore the precipitation event corresponding to peak IV is due to β-cubes and Si precipitates. The broad endothermic peak V is caused by the dissolution of β-cubes and Si precipitates.

In Fig. 6 the DSC plots for the as-quenched and shock-loaded samples are displayed. As can be seen, while the occurrence temperature of peaks I and II and peaks I′ and II′ look similar in both the shock-loaded and un-shocked samples, the temperature formation of peaks III′ and IV′

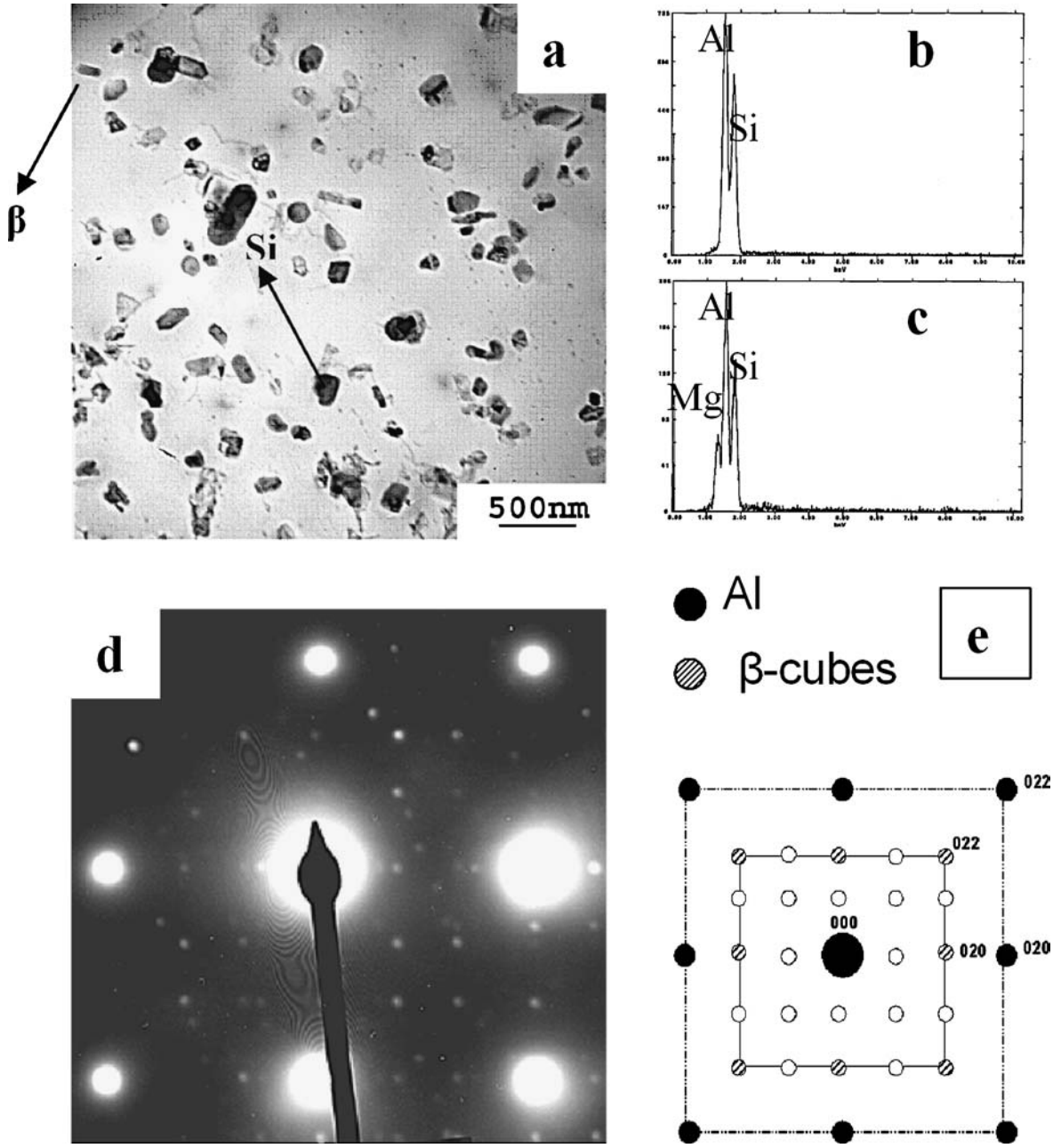

Figure 5 (a) The microstructure of the sample heated to peak IV with heating rate of 10°C/min. The EDS analysis indicates that the precipitates are (b) Si and (c) β. (d) $<100>_{Al}$ diffraction pattern corresponds to microstructure (a). (e) Schematic of the diffraction pattern (d).

in Fig. 6b is lower than peaks III and IV in Fig. 6a. To investigate the DSC results in more detail, TEM studies were performed on the samples heated to peaks I′, II′, III′ and IV′ respectively. Conventional TEM analysis on peak I′ revealed no distinct precipitates in the microstructure and thus similar to the argument given for peak I, it was assumed that the peak I corresponds to clustering/GP zone formation. The heat of reaction corresponding to peaks I and I′ looks similar which means that shock-loading prior to dynamic heating did not affect the formation of clustering/GP zones.

Fig. 7 corresponds to the bright field TEM micrograph and SAD pattern of the alloy heated up to 230°C (peak II′). Similar to Fig. 3, the needle-shaped precipitates are seen in the matrix parallel to the $<100>_{Al}$ zone axis of the matrix (Fig. 7a). The morphology of the precipitates and the symmetrical faint streaks in the SAD pattern (Fig. 7b) suggest that these precipitates are β''. Close examination of the end-on precipitates shows that in addition to the needle-shaped precipitates, small lath shaped precipitates are also present. Therefore peak II′ is characterized to be due to the formation of β'' and lath-shaped precipitates. By comparing the precipitates in peaks II and II′, one can conclude that the pre-shock loading did not have any significant effect on the nature of β'' and lath-shaped precipitates formation.

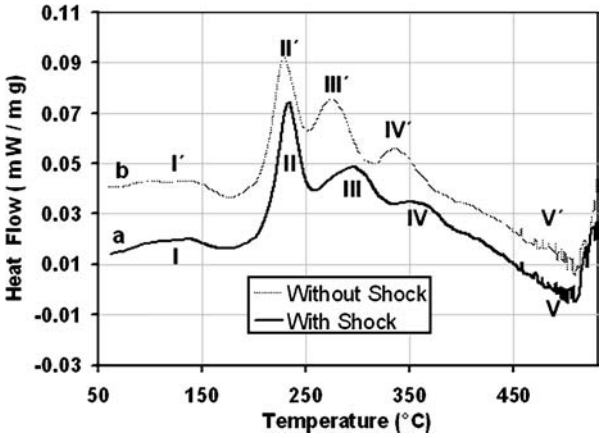

Figure 6 DSC curves at a heating rate of 10°C/min for samples (a) as-quenched condition (b) shock-loaded prior to DSC run.

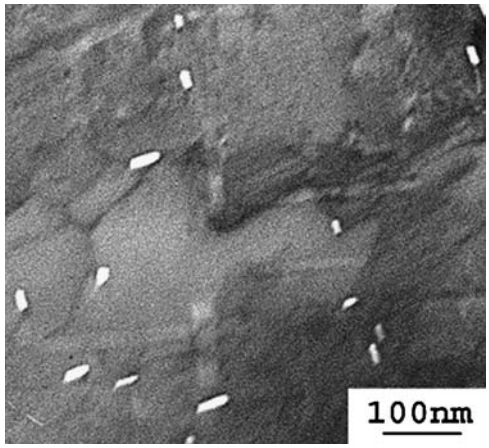

Figure 9 The $<100>_{Al}$ TEM dark field micrograph of the microstructure of shock-loaded sample after the occurrence of peak III′.

Fig. 8 shows the bright field TEM image and SAD pattern of the precipitates after the occurrence of peak III′. Although it seemed that rod-like or needle-like precipitates with different diameters were observed along $[010]_{Al}$ and $[001]_{Al}$ directions, close examination of the end-on precipitates revealed that most of them were rectangle-shaped. This can be seen clearly in the TEM dark field image of this sample (Fig. 9). Diffraction pattern and analyses of the end-on precipitates in the dark field TEM

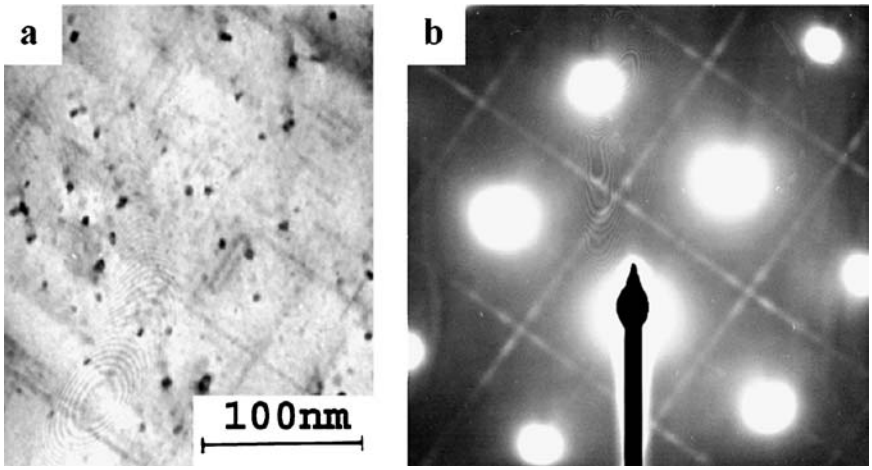

Figure 7 The microstructure of the sample shock-loaded prior to DSC heating experiment after the occurrence of peak II′ (a) Bright field imaging (b) SAD pattern at $<100>_{Al}$ zone axes.

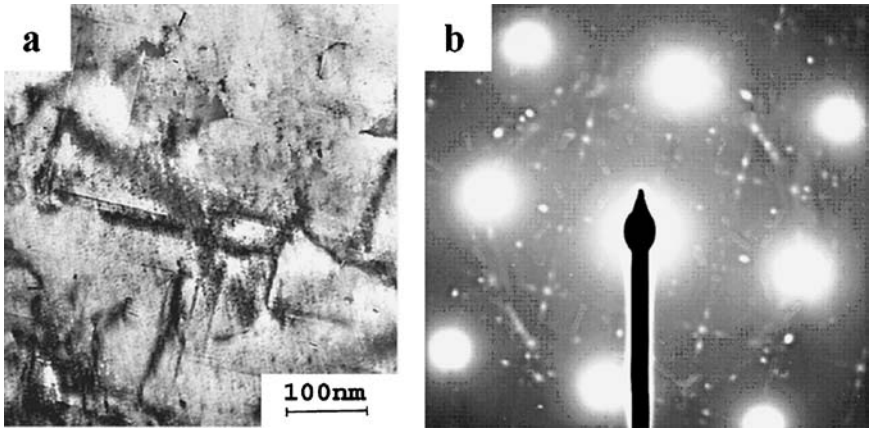

Figure 8 The microstructure of the sample shock-loaded prior to the DSC heating experiment after the occurrence of peak III′ (a) Bright field imaging (b) SAD pattern at $<100>_{Al}$ zone axes.

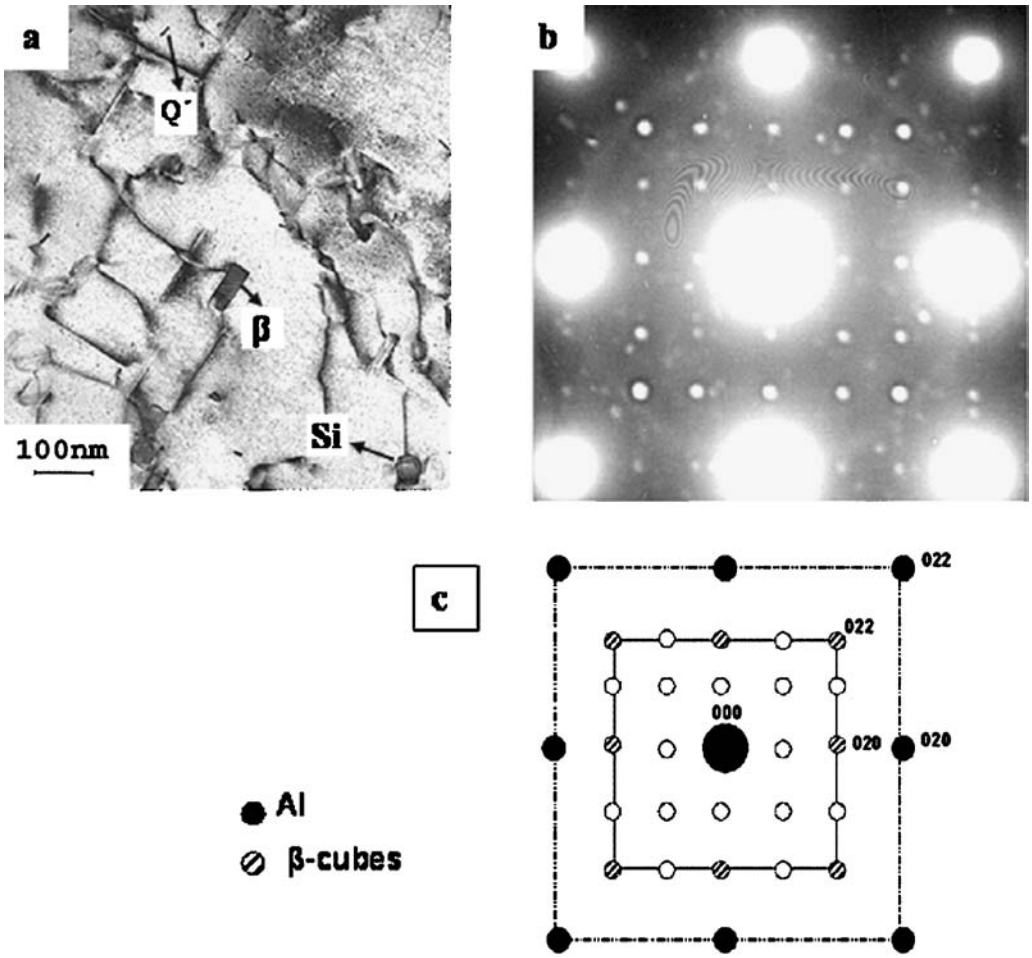

Figure 10 The microstructure of shock-loaded sample heated to peak IV′ (∼330°C) (a) The dark field micrograph shows β-cubes (b) The diffraction pattern including $<100>_{\beta-\text{cubes}}$ and $<100>_{\text{Al}}$ (c) The schematic representation of (b).

image, suggests that the rectangle-shaped precipitates are Q'. It is interesting to note that while the peak III in the un-shocked sample corresponds to β' and Q', the exothermic peak III′ is due to the formation of Q' precipitates. In a previous study [26], we observed similar behavior of the pre-deformed samples. This also agrees well with high resolution TEM analyses of Matsuda *et al*. [27]. His studies showed that Type-C precipitates (similar to Q' phase) were typical in the deformed Al-Mg-Si alloys containing excess Si. Therefore the precipitation event corresponding to peak III′ on the DSC trace of Fig. 6b can be characterized to be due to the precipitation of Q'.

The bright field image, the SAD pattern and the key diagram for the microstructure corresponding to the sample heated to 330°C (peak IV′) are shown in Fig. 10a, 10b and 10c. The presence of Q' phase can be recognized in the bright field image shown in Fig. 10a. The diffraction pattern (Fig. 10b) and its analysis (Fig. 10c) indicate that, similar to the un-shocked samples, the β-cubes are present and related to the matrix by the orientation relationship:

$$[001]_{\text{ß}-\text{cubes}}||[001]_{\text{Al}}, \quad [100]_{\text{ß}-\text{cubes}}||[100]_{\text{Al}},$$
$$[010]_{\text{ß}-\text{cubes}}||[010]_{\text{Al}}$$

EDS analyses reveal that in addition to β particles, Si precipitates were also present in the microstructure. Therefore peak IV′ corresponds to the formation of β-cubes, Q' and Si precipitates. In contrast to peak IV in the un-shocked sample, the Q' phases are present in this precipitation event, and the peak temperature in

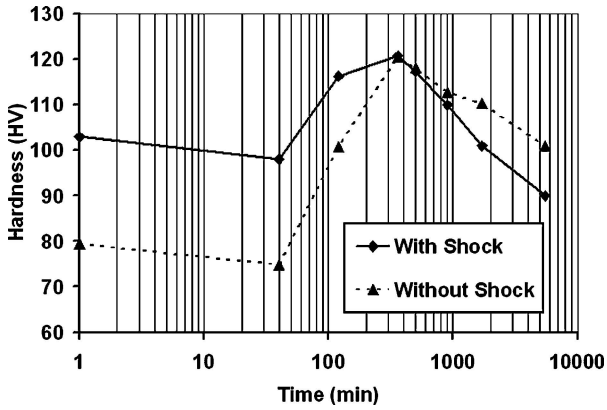

Figure 11 Dependence of hardness on artificial aging time at 175°C. (a) without shock-loading (b) with shock-loading.

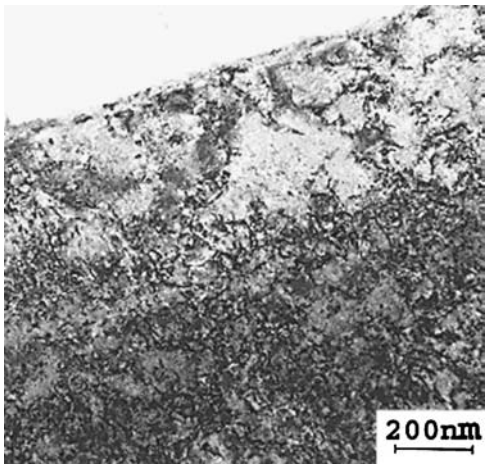

Figure 12 The microstructure of AA6022 after being quenched from solutionizing temperature and subsequently shock-loaded to 23 GPa.

the shock-loaded sample is shifted to lower temperature by ~50°C.

The age-hardening behavior of the shock-loaded AA6022 samples was also studied. Fig. 11 shows the hardness as a function of artificial aging time for samples with and without shock-loading at a temperature of 175°C. At the early stage of aging the hardness of the shock loaded sample is significantly higher than the un-shocked sample due to high dislocation density and other microstructural defects produced after shock-loading (Fig. 12). At later stages of aging the hardness of both the shocked and un-shocked samples becomes closer and eventually both samples reach the same hardness value after 400 min aging at 175°C (peak of hardness). For further details, TEM analyses were performed on both samples at the peak of hardness and the results are shown in Fig. 13. According to the diffraction pattern and close examination of the end-on precipitates, precipitates in both samples were characterized as needle-like, β'', and lath- shaped precipitates as majority and minority phases, respectively. Note that β'' precipitates are the major precipitates responsible for the observed maximum hardness in both shocked and un-shocked samples. This agrees well with other studies on aging behavior of Al-Mg-Si alloys which show that β'' precipitates are major precipitates associated with the peak of aging [19, 27, 28]. Therefore one may conclude that pre-shock loading treatment did not have any significant effect on the peak of hardness and associated precipitates.

The effect of shock-loading becomes more pronounced in the overaged condition. According to Fig. 11, in the overaged condition, the hardness in the shock loaded sample decreases faster in comparison to the un-shocked material. This behavior is consistent with the DSC re-

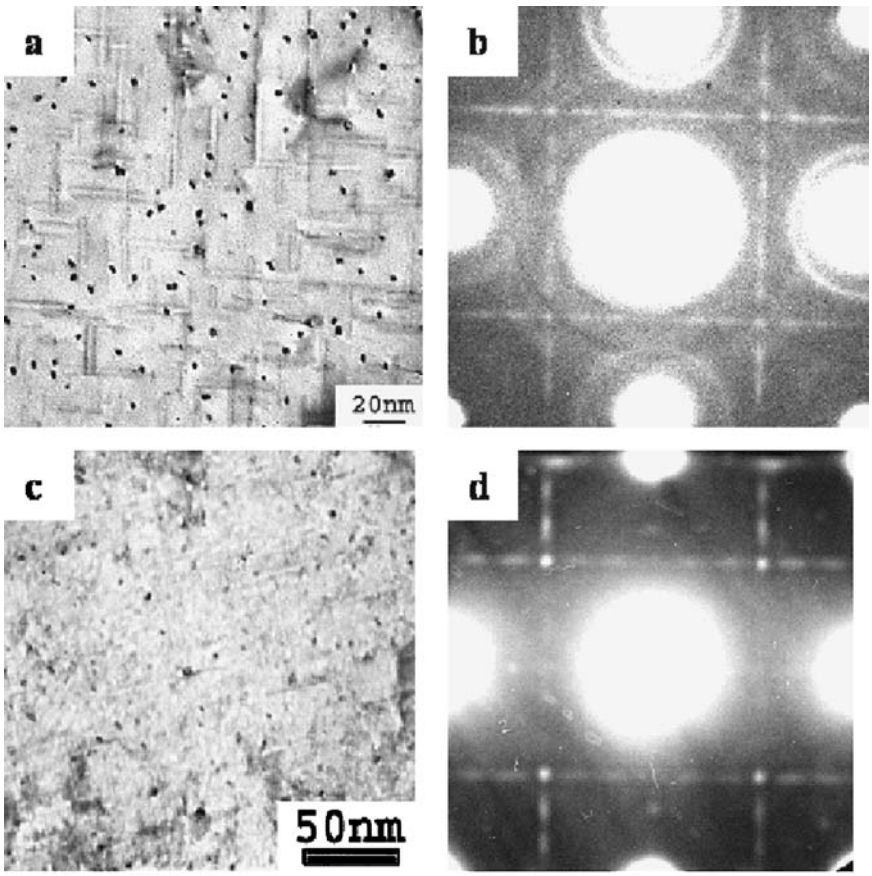

Figure 13 Bright field imaging and SAD pattern at $<100>_{Al}$ zone axes of the microstructure of the AA6022 aged at 175°C for 500 min (a-b) without shock (c-d) with shock.

sults of shock-loaded material (given in Fig. 6b) where the acceleration of peaks III′ and IV′ was observed. The DSC results and isothermal aging behavior of pre-shock loaded samples suggest that shock-loading more likely affects the phases closer to the equilibrium state (i.e. β', Q' and β phases rather than the clusters/GP zones and β'' precipitates). As can be seen, the precipitation of β'' happens immediately after the formation of GP zones which suggests that β'' nucleates on GP zones. More detailed analyses performed by Murayama and Hono [12] confirm that GP zones provide heterogeneous nucleation sites for the β'' precipitates. Also the atomic probe field ion microscopy (APFIM) studies of Edwards *et al.* [13] on Al-Mg-Si alloys show that the distribution of intermediate phases strongly depends upon the distribution of co-clusters. Therefore, one can conclude that the precipitation of β'' more likely depends on clustering/GP zones rather than other microstructural defects. According to the DSC results, shock-loading did not have any significant influence on the formation of clusters/GP zones (see peak I and I′ in Fig. 6). Therefore, it is reasonably expected that the precipitation reaction corresponding to β'' would not change either. That is why in both the shocked and un-shocked samples the exothermic peak due to β'' precipitation was at a similar position (see peaks II and II′ in Fig. 6). However after the β'' precipitates form, the formation rate of the subsequent phases can be affected by the presence of these microstructural defects produced due to the shock process. The reason can be explained by the fact that β' and Q' form due to the growth of β'' precipitates [15, 24]. The presence of a large density of dislocations and other microstructural defects accelerates the growth rate of β''. These defects may act as rapid diffusion paths for transferring the solute atoms from the bulk to the β'' precipitates, and thus the kinetics of β' and Q' formations become faster in comparison to the un-shocked sample. It is also interesting to note that while in the un-shocked sample (Fig. 4), both rod-like β' and lath-like Q' precipitates are present, in shock-loaded samples (Figs. 8 and 9) only Q' precipitates are seen. The Q' phase was even co-existed with equilibrium phases, β and Si (Fig. 10). Therefore, one can conclude that the presence of dislocations preferentially promotes the formation of the Q' phase over the β' phase. It should be noted that both β' and Q' phases have hexagonal crystal structure, and such a promotion may not be predictable. However, it can be explained by the fact that the habit plane of Q' has been determined to be $\{150\}$ of the aluminum matrix [23]. The repeat distance along the <150> directions of the aluminum matrix is 1.03 nm which is about the same as the lattice parameter of the Q' phase [22, 23]. Therefore the precipitates tend to form as a lath so as to minimize the misfit in its surface and hence its energy. In fact, similar observations have been reported by Deschamps *et al.* [29] and Ringer *et al.* [30]. Ringer *et al.* [30] showed that despite similarities in the morphology and crystallography of Ω and T_1 phases, cold-working prior to aging promoted the precipitation of T_1 in an Al-Cu-Li-Mg-Ag alloy and decreased the density of Ω phases in an Al-Cu-Mg-Ag alloy.

4. Conclusions

The impact of shock-loading on the precipitation reaction in an Al-0.55%Mg-1.10%Si-0.06 wt% Cu was studied by means of DSC, TEM and hardness tests. The shock-loading prior to aging altered the formation temperature and the nature of the precipitation sequence in this alloy. The following conclusions were made:

1. TEM analyses on DSC peak II′ and the peak of hardness state revealed that shock-loading did not have any significant impact on the β'' precipitates. This suggests that the formation of β'' precipitates highly depends on the GP zones rather than other microstructural defects.
2. In the overaged condition, the shock-loaded sample showed faster hardness reduction in comparison to an un-shocked sample. TEM analyses revealed that shock-loading accelerated the rate of formation of overaged precipitates, Q' and β.
3. TEM analyses on the DSC peaks III and III′ revealed that the precipitates in the un-shocked sample were $\beta'+Q'$, and the precipitates in the shocked sample were Q'.

Acknowledgments

The authors gratefully acknowledge Kent Perkins, for preparing and operating the ISP gun facility, Dave Savage for preparation of the samples, and Kurt Zimmerman for advice on fixture design. Also thanks to Dr. M. Laborie at Washington State University for her assistance with DSC experiments.

References

1. C. S. SMITH, *Trans. AIME* **212** (1958) 574.
2. J. R. ASAY, G. R. FOWLES, G. E. DUVALL, M. H. MILES and R. F. TINDER, *J. Appl. Phys.* **43** (1972) 2132.
3. M. A. MEYERS, in "Dynamic Behavior of Materials" (John Wiley & Sons, New York, 1994) 382.
4. L. E. MURR, in Proceeding of an international conference on metallurgical effects of high-strain-rate deformation and fabrication, Albuquerque, June 1980, edited by M. A. Meyers and L. E. Murr (Plenum, New York, 1981) p. 306.
5. G. T. GRAY III, in "High Pressure Shock Compression of Solids," edited by J. R. Asay and M. Shahinpoor (Springer-Verlag, New York, 1993) p. 118.
6. L. DAVISON and R. A. GRAHAM, *Physics Report* **55** (1979) 255.
7. L. E. MURR, in "Shock Waves in Condensed Matter," edited by S. C. Schmidt and N. C. Holmes (Amsterdam, New York, 1988) p. 230.
8. R. ESQUIVEL and O. T. INAL, *J. Mater. Sci.* **30** (1995) 5825.
9. A. I. UVAROV, V. I. ZELDOVICH, O. S. RINKEVICH and I. N. GAVRILEV, *Phys. Metals Metallog.* **83** (1997) 199.
10. A. N. BEKRENEV and L. A. NAUMOV, *Phys. Metals* **6** (1985) 707.

11. I. DUTTA and S. M. ALLEN, *J. Mater. Sci. Lett.* **10** (1991) 323.
12. M. MURAYAMA and K. HONO, *Acta Mater.* **47** (1999) 1537.
13. G. A. EDWARDS, K. STILLER, G. L. DUNLOP and M. J. COUPER, *Acta Mater.* **46** (1998) 3893.
14. S. J. ANDERSEN, H. W. ZANDBERGEN, J. JANSEN, C. TRÆHOLT, U. TUNDAL and O. REISO, *Acta Mater.* **46** (1998) 3283.
15. M. H. JACOBS, *Phil. Mag.* **26** (1972) 1.
16. Y. OHMORI, L. C. DOAN, Y. MATSUURA, S. KOBAYASHI and K. NAKAI, *Mater. Trans.* **42** (2001) 2576.
17. L. DAVISON and R. A. GRAHAM, *Physics Report* **55** (1979) 255.
18. T. ANTOUN, L. SEAMAN, D. R. CURRAN, G. I. KANEL, S. V. RAZORENOV and A. V. UTKIN, in "Spall Fracture," edited by L. Davison and Y. Horie (Springer-Verlag, New York, 2003) p. 63.
19. W. F. MIAO and D. E. LAUGHLIN, *Metal. Mater. Trans. A* **31** (2000) 361.
20. A. K. GUPTA and D. J. LLOYD, *ibid.* **30** (1999) 879.
21. M. MURAYAMA, K. HONO, W. F. MIAO and D. E. LAUGHLIN, *ibid.* **32** (2001) 239.
22. D. J. CHAKRABARTI and E. LAUGHLIN, *Progress in Mater. Sci.* **49** (2004) 389.
23. S. D. DUMOLT and D. E. LAUGHLIN, *Scripta Mater.* **18** (1984) 1347.
24. W. F. MIAO and D. E. LAUGHLIN, *ibid.* **40** (1999) 873.
25. H. WESTENGEN and N. RYUM, *Z. Metallkunde.* **70** (1979) 528.
26. R. S. YASSAR, D. P. FIELD and H. WEILAND, *Scripta Mater.* 2005, (In Press).
27. K. MATSUDA, S. SHIMIZU, H. GAMADA, Y. UETANI, F. SHINAGAWA and S. IKENO, *J. Soc. Mat. Sci. Japan* **48** (1999) 10.
28. A. K. GUPTA, D. J. LLOYD and S. A. COURT, *Mater. Sci. Eng. A* **301** (2001) 140.
29. A. DESCHAMPS, F. LIVET and Y. BRÉCHET, *Acta Mater.* **47** (1999) 281.
30. S. P. RINGER, B. C. MUDDLE and I. J. POLMEAR, *Metal. Mater. Trans. A* **26** (1995) 1659.

Received 23 March
and accepted 9 June 2005